scientific reports

Check for updates

OPEN

Computational study of skyrmion stability and transport on W/CoFeB

Tsz Chung Cheng✉, Lin Zhang, Yuichiro Kurokawa, Ryuta Satone, Kazuhiko Tokunaga & Hiromi Yuasa

Skyrmions are topologically protected magnetic structures originating from Dzyaloshinbskii–Moriya Interaction (DMI) which can be driven by a spin-polarized current making it a candidate for many different novel spintronic devices. However, the transport velocity is proportional to the size of the skyrmion rendering the effort of miniaturizing spintronics devices useless indicating that it is not possible to realise high-speed transport, small size and low operating current at the same time. One approach to solving the trilemma is to increase the spin Hall angle θ_{SH}, the conversion ratio between charge current and spin current, in the heavy metal layer. For example, beta-tungsten (β -W) has attracted attention due to its high spin Hall angle, abundance in nature and the potential to combine with other materials to form complex structures. To characterise the use of β-W as a heavy metal layer along with a CoFeB magnetic layer, the interfacial DMI and the external field required to generate skyrmions were estimated to be 1.5 $\mathrm{mJ/m^2}$ and 0.1 T respectively, which were confirmed to be realistic. In that case, the about 10 nm diameter skyrmion was transported under SOT at a velocity of about 40 m/s, which has the potential for skyrmion-based unconventional computing devices like skyrmion race track memory and logic gate.

The rapid advancements in artificial intelligence and big data applications have underscored the critical need for storage solutions that offer a compelling combination of high density, exceptional performance, energy efficiency, robust reliability, and enhanced security. Skyrmions, a topologically non-trivial magnetic nanostructure, can be stored in high density and transported at a high velocity with little power[1–3]. These advantages attracted research into skyrmion racetrack memory, skyrmion logic devices, artificial synapses, and other devices[4–8]. Skyrmions can be generated by the interfacial Dzyaloshinskii-Moriya Interaction (DMI) arising from a spatial symmetry breaking at the interface between ferromagnetic and heavy metal layers. The Hamiltonian of the DMI between two neighbouring spins, $\mathbf{S_1}$ and $\mathbf{S_2}$ can be characterized by:

$$\hat{\mathscr{H}}_{DM} = -\mathbf{D_{12}} \cdot (\mathbf{S_1} \times \mathbf{S_2}) \tag{1}$$

under the DMI vector $\mathbf{D_{12}}$ characterized by the heavy metal layer. As a result, the two spins do not align parallel or anti-parallel favoured by exchange interaction. To minimize the energy in such a symmetry broken and PMA system, a possible ground state is to generate a skyrmion when a balance exists between the DMI, PMA, exchange and demagnetisation energy[9–12]. Skyrmion has been observed in heavy metal and ferromagnetic multilayers such as $[\mathrm{Ir/Fe/Co/Pt}]_{20}$[13], $[\mathrm{Ir/Co/Pt}]_{10}$[14], Pt/Co/Os/Pt[15], Pt/Co/Ta[16], Pt/CoFeB/MgO[17], Ta/CoFeB/MgO[18] and W/CoFeB/MgO[19]. For the latter three CoFeB systems, the interfacial DMI constant $D_{interfacial}$ were found to be within the same range. It was suggested that a W/CoFeB system has the same interfacial DMI constant $D_{interfacial} = 1.15 \pm 0.57\ \mathrm{mJ/m^2}$ as a Pt/CoFeB system within the uncertainties of measurements[20]. Another piece of work used a different structure Pt/Co/X (X can be W or other materials like Ti and Ta). For W, $D_{interfacial} = 1.48 \pm 0.03\mathrm{mJ/m^2}$ is comparable with materials such as Cu and Ti while being higher than Ta[21]. The W/CoFeB caught the attention because of W's abundance in nature and the ability to form multilayers or alloys with other materials to tailor the desired material parameters such as DMI constant, spin Hall angle and resistivity[22–28].

To realize low-power and high-density spintronic devices based on skyrmions, skyrmions have to be transported to act as an information carrier. In this process, spin orbit torque (SOT) can be utilized to transport or manipulate the skyrmion, which can conveniently be generated from the heavy metal layer already in the system[29–31]. However, there exists a trilemma in the transport velocity v of a skyrmion,

Graduate School of Information Science and Electrical Engineering, Kyushu University, Fukuoka 819-0382, Japan. ✉email: jed.cheng@mag.ed.kyushu-u.ac.jp

$$v \propto \frac{d \times J \times \theta_{SH}}{M_{sat} \times t} \tag{2}$$

where the transport velocity v is proportional to the diameter of the skyrmion d, the current density J and the heavy metal layer's spin Hall angle θ_{SH}, while inversely proportional to the magnetic layer's saturation magnetisation M_{sat} and thickness t[32–35]. The proportionality of the skyrmion diameter and transport velocity hinders the effort of miniaturising skyrmion devices.

One can improve the effective SOT efficiency by decreasing the M_{sat} and the thickness of the magnetic layer to overcome the problem. Approaches like using ferrimagnetic or antiferromagnetic materials and designing synthetic antiferromagnetic (SAF) structures can be employed to decrease M_{sat}[36]. Skyrmions in ferrimagnets composed of rare earth and transition metals are being actively studied because the momentum compensation can reduce the magnetisation and the angular momentum compensation improves SOT efficiency[37,38]. However, the angular momentum compensation temperature is typically so close to the device operating temperature that stable and desired magnetic properties are hard to obtain[39,40]. Skyrmions in antiferromagnets[41,42] and SAF structures[43–45] have no net magnetisation so as skyrmion Hall effects making them an attractive candidate for skyrmion transport. Unfortunately, these structures only have Néel vectors making it difficult to detect skyrmions using magnetoresistance when designing and constructing a device.

On the other hand, one could leverage θ_{SH} of the heavy metal layer to overcome the trilemma of velocity and diameter without a dramatic change to magnetic properties when using ferrimagnetic or antiferromagnetic materials. A promising material is tungsten in its β form (β-W) that can provide θ_{SH} in the range of -0.30 to -0.49[46–51]. In contrast, other commonly used materials such as Platinum *Pt* only have a θ_{SH} ranging from 0.03 to 0.10[52–57]. Recent work focused on alloying β-W with materials such as Ti[58] to achieve lower resistivity and higher θ_{SH}. Another work introduced N as a dopant to suppress the formation of α-W while promoting β-W to further increase the spin Hall angle showcasing the enormous potential of β-W in SOT devices[59]. Even larger values of spin Hall angles up to 0.8–0.9 have been reported[60] suggesting further the potential for future iterations and improvements. Compared to the other approaches, increasing θ_{SH} is the most realistic way to enhance SOT as the high θ_{SH} in β-W may increase the skyrmion transportation velocity and overcome the trilemma in skyrmion transport.

In this work, the skyrmion generation conditions in terms of the external field and DMI constants in a β-W/CoFeB system were characterized. The results would provide a window of the conditions required to generate skyrmions in a β-W/CoFeB system. Since skyrmions are a result of the balance between DMI, PMA, exchange and demagnetisation energy, their size is expected to change with the external field $B_{z,ext}$and interfacial DMI constant $D_{interfacial}$. The sizes of the skyrmion are correlated with the transport velocity of the skyrmion as suggested leading to the second part of the study. The generated skyrmions were transported under SOT with different spin Hall angles θ_{SH} to verify the effect of θ_{SH} on the transport velocity of small-sized skyrmions. The correlation between these factors in both the first and second parts can provide useful insight for future material and device engineering that requires precise control of aspects such as skyrmion size and transport velocity.

Results and discussion

This computational study is divided into three parts. The first part determined the initial state of the skyrmion generation process forming the basis of the other simulations. The $D_{interfacial}$ and $B_{z,ext}$ required to generate skyrmions were then characterized using the initial conditions determined. It is followed by a study into the transport behaviour from SOT under different spin Hall angles θ_{SH}. The detailed configuration of the finite different micromagnetic simulator Mumax3, which solves the Landau-Lifshitz-Gilbert equation, can be found in the Methodology section[61].

Initial states

The generation of skyrmion was achieved by applying a uniform field in the −z-direction against an initial magnetisation state during a relaxation process. Since the results could be heavily influenced by the initial state, three initial magnetisation states were considered:

1. a random magnetisation
2. a uniform magnetisation in +z-direction
3. a uniform magnetisation in −z-direction with a −z-direction magnetisation circular region in the middle

As shown in Fig. 1a–c respectively. To test out the three initial states, simulations were conducted with $D_{interfacial} = 1.5\text{mJ}/\text{m}^2$ and $B_{z,ext} = 0.1$ T. For State (1), a random initial magnetisation, multiple Néel-type skyrmions were formed on the mesh as shown in Fig. 1d. The typings were determined by in-plane components pointing away from the centre of the skyrmion[62]. Stripe domain walls, on the other hand, were formed from State (2) which can be found in Fig. 1e. Figure 1f shows the relaxed state of State (3), where a single Néel-type skyrmion was formed after the relaxation. A random State (1) can easily generate a lot of skyrmions compared to the other two configurations. It is possible to achieve a random magnetisation state by heating the sample above the Curie temperature T_c and cooling it under an external field known as the field cool method[63–65]. However, the W/CoFeB/MgO system of 1.2 nm thickness of CoFeB was reported to have a T_c up to 750 K[66]. The high T_c renders the method impractical for experiments. State (3), a circular region with anti-parallel uniform magnetisation in the middle is also in-practical for experiments. On the other hand, in State (2),

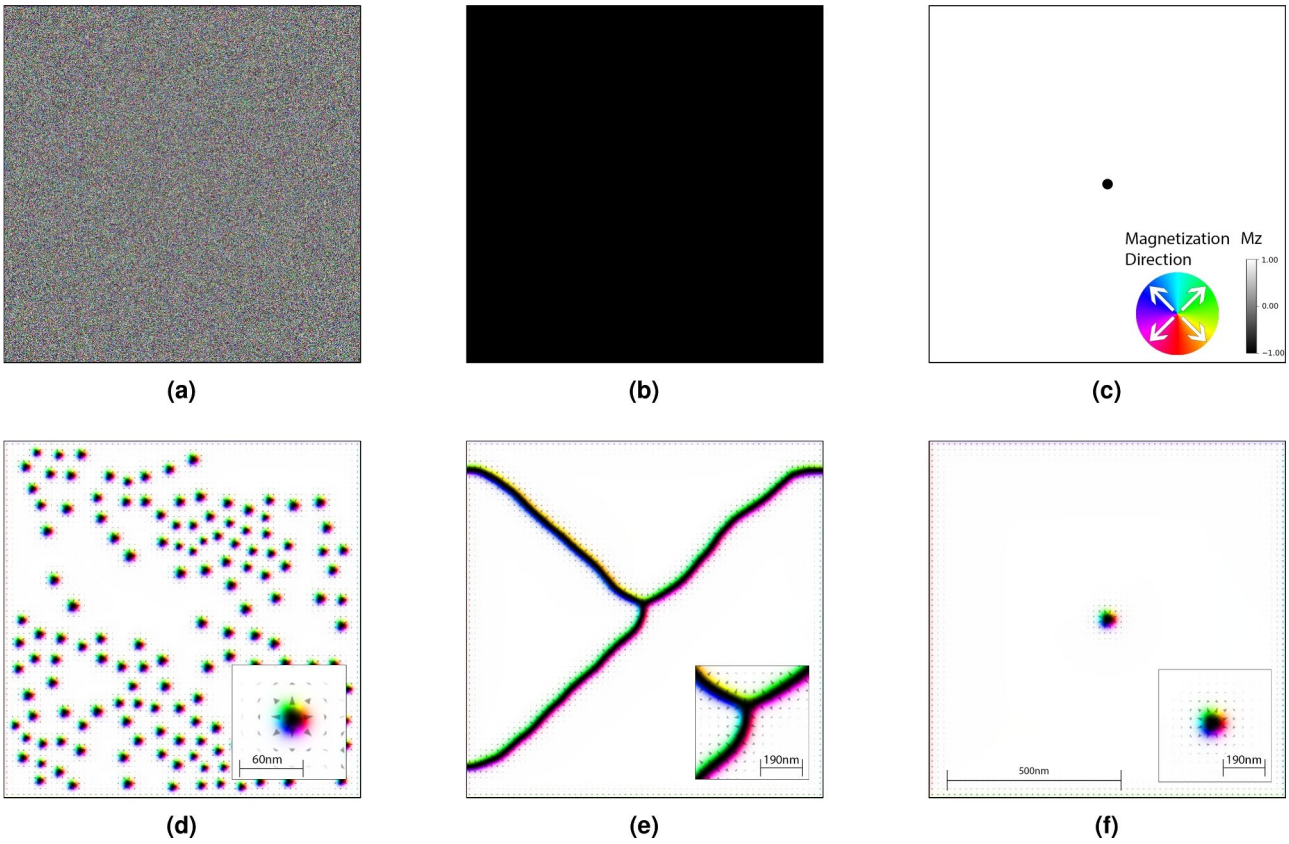

Fig. 1. Three different initial states considered. (**a**) A random magnetisation, (**b**) a uniform magnetisation in +z-direction and (**c**) a uniform magnetisation in −z-direction but a -z-direction magnetisation circular region 30 nm diameter in the middle. (**d**–**f**) The resultant states after relaxation under $D_{interfacial} = 1.5\mathrm{mJ/m^2}$ and $B_{z,ext} = 0.1$ T for the three initial states respectively. The inserts show the feature of each relaxed state, corresponding to Néel skyrmions in (**d**) and (**f**) but Néel stripe domain walls in (**e**).

a uniform magnetisation in ±z-direction can be easily generated by applying a saturation field, although it was more difficult to generate skyrmions. Thus it was chosen as the initial state for this study.

Skyrmion generation criteria and resultant diameter

Under the chosen initial state, for the skyrmion generation process, $B_{z,ext}$ ranging from 0 to 0.2 T was applied under $D_{interfacial}$ ranging from 0 to 2.0 $\mathrm{mJ/m^2}$. Figure 2 shows results from the skyrmion generation part of the study indicating the relaxed state under different $D_{interfacial}$ and $B_{z,ext}$. It can be divided into four categories, an un-flipped magnetisation, a flipped magnetisation, a skyrmion and stripe domain walls. As the external field $B_{z,ext}$ increased, the Zeeman energy overcame the PMA and the magnetisation was flipped. It allowed the observations of the DMI field exerted on the system. If the DMI energy was sufficient, domain walls were formed to minimize overall energy. With the continued increase of $B_{z,ext}$, at 0.08 T and $D_{interfacial} = 1.1\mathrm{mJ/m^2}$, a skyrmion was generated. It is a point where the equilibrium between DMI, PMA and the external field which is also the minimum $D_{interfacial}$ and $B_{z,ext}$ required to generate skyrmion in this system. Assuming K_u is unchanged, the range of uncertainties in the value $D_{interfacial} = 1.15 \pm 0.57\mathrm{mJ/m^2}$ from[20] might fall into the region lower than $D_{interfacial} = 1.0$ mJ and not able to generate a skyrmion. On the other hand, it could fall into the upper range of forming a stripe domain wall pattern. In this case, an increase in $B_{z,ext}$ would be required to transit into a skyrmion ground state.

Nonetheless, the region of which skyrmions were generated expanded with the increase in $B_{z,ext}$. The same trend could also be seen from the pattern of the stripe domain walls. Focusing on the cases of $D_{interfacial} = 2.0\mathrm{mJ/m^2}$. Even at $B_{z,ext} = 0.0$ T, the DMI was able to overcome the PMA and flipped part of the mesh's magnetisation to form complex stripe domain wall structures. The increase in Zeeman energy gradually reduced the complexity of the stripe domain walls. Eventually, the complex stripe domain walls were reduced to a skyrmion at $B_{z,ext} = 0.13$ T. One could notice that at $B_{z,ext} = 0.20$ T, the skyrmion was not situated in the centre of the mesh. The high Zeeman energy in this case resulted in a rapid shrinking of domain walls which the symmetry of the process was distorted by the grains in the system. The video of the generation process at $B_{z,ext} = 0.15$ T and 0.20 T were included in Supplementary Material 1 and 2 respectively.

Within the skyrmion favourable parameter space, the size of the generated skyrmions changes. To obtain the size of the resultant skyrmions, the following formulation was used:[67]

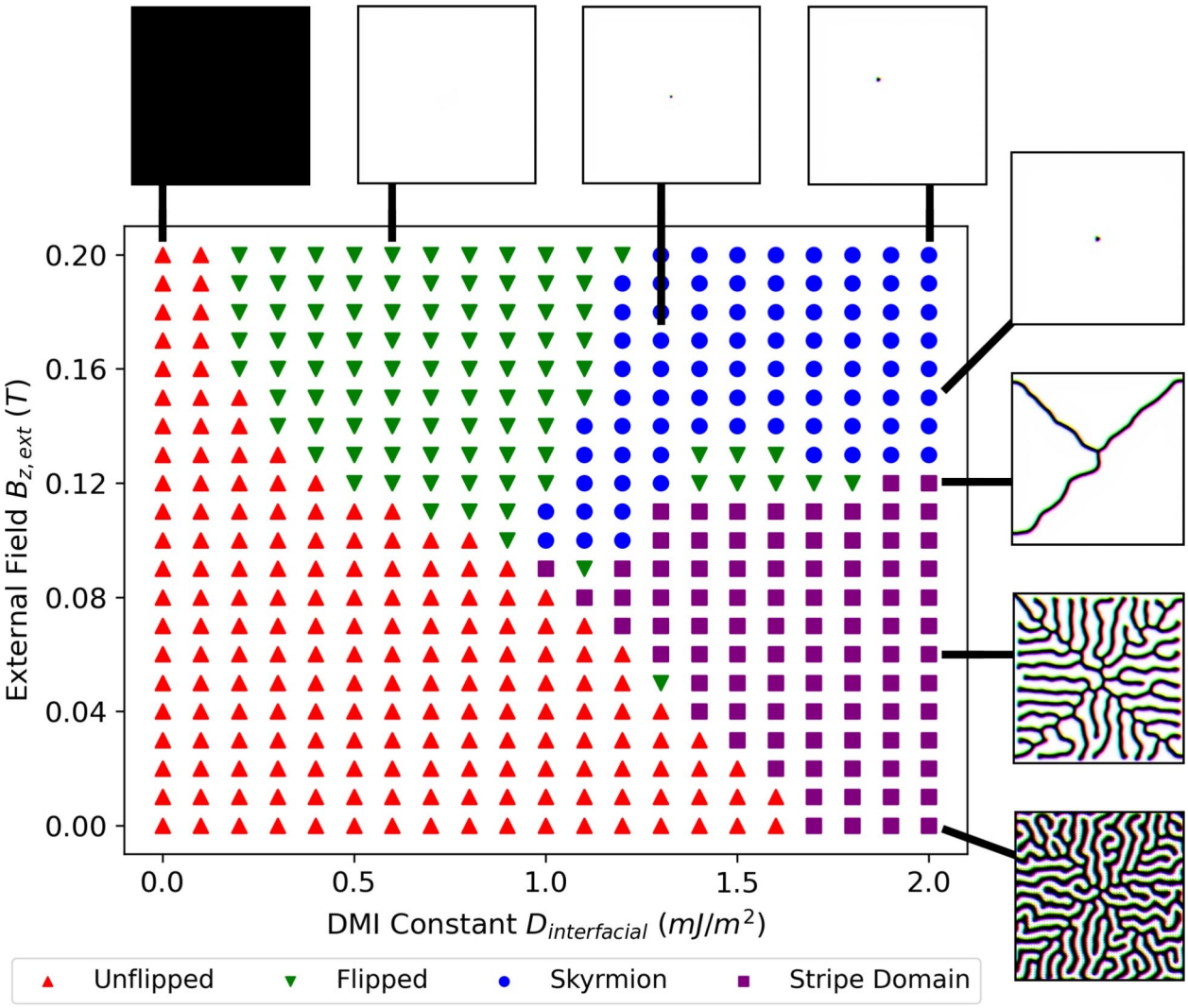

Fig. 2. Map indicating different relaxed ground states which the system evolved into including an unflipped state, a flipped state, a skyrmion and domain wall across different $B_{z,ext}$ and $D_{interfacial}$. The inserts show an example for each state. Focusing on the $D_{interfacial} = 2.0\mathrm{mJ/m}^2$ case, as $B_{z,ext}$ increases, the domain wall structures become less complex and form a skyrmion at $B_{z,ext} = 0.13$ T.

$$\Theta(r) = 2arctan\left[\frac{sinh(R/w)}{sinh(r/w)}\right] \tag{3}$$

where the polar angle of the magnetisation Θ at point r away from the centre of the skyrmion is given by the radius R and 360° domain wall width w. The formulation fits well into the generated skyrmions, despite noticeably a lack of a plateau around the centre of the skyrmion generated under $B_{z,ext} = 0.14$ T and $D_{interfacial} = 2.0$ $\mathrm{mJ/m}^2$ as shown in Fig. 3a. The diameter of the resultant skyrmion decreased with increasing $B_{z,ext}$ which can be explained by the increase in Zeeman energy as shown in the heat map in Fig. 3b. On the other hand, the opposite trend could be seen with the increase of DMI constants increasing the skyrmion radius. It is due to the presence of a negative sign in DMI energy contribution to the total energy. Recently, the various topological structures were studied, expanding the possibility of skyrmion properties and usage. For example, by repeating Ta/CoFeB/MgO layers, a magnetic structure different from a simple skyrmion, called a skyrmion bag, can be obtained[68]. In such a structure, the skyrmion size reaches the micrometre range mainly due to the large demagnetization field[19,69], suggesting the single W/CoFeB/MgO layer is preferable to reduce the size of skyrmion.

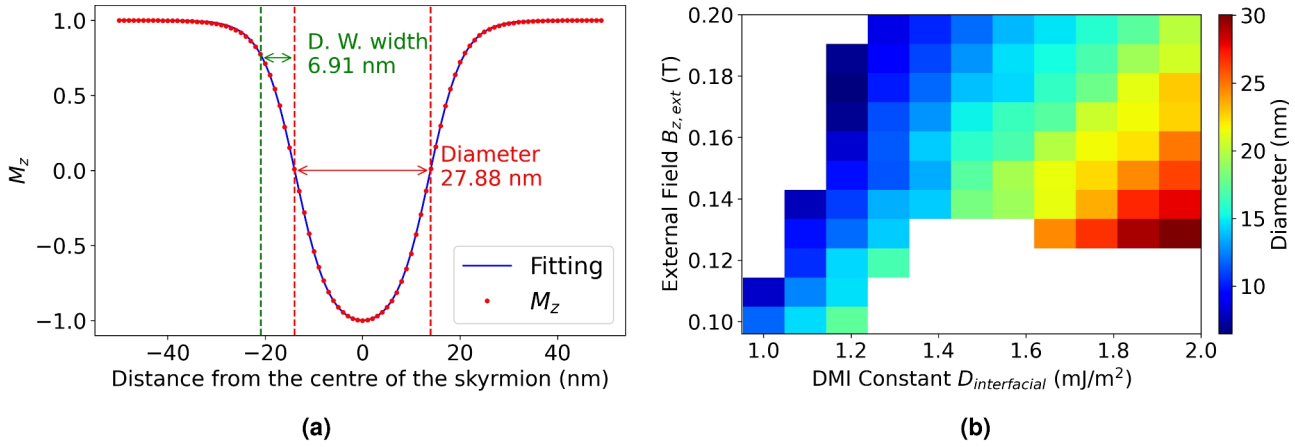

Fig. 3. (**a**) Cross section M_z of a skyrmion generated under $B_{z,ext} = 0.14$ T and $D_{interfacial} = 2.0\text{mJ/m}^2$. The fitting results suggest the skyrmion has a diameter of 27.88 nm and a domain wall width of 6.91 nm. (**b**) The size of the skyrmions generated different conditions of $B_{z,ext}$ and $D_{interfacial}$.

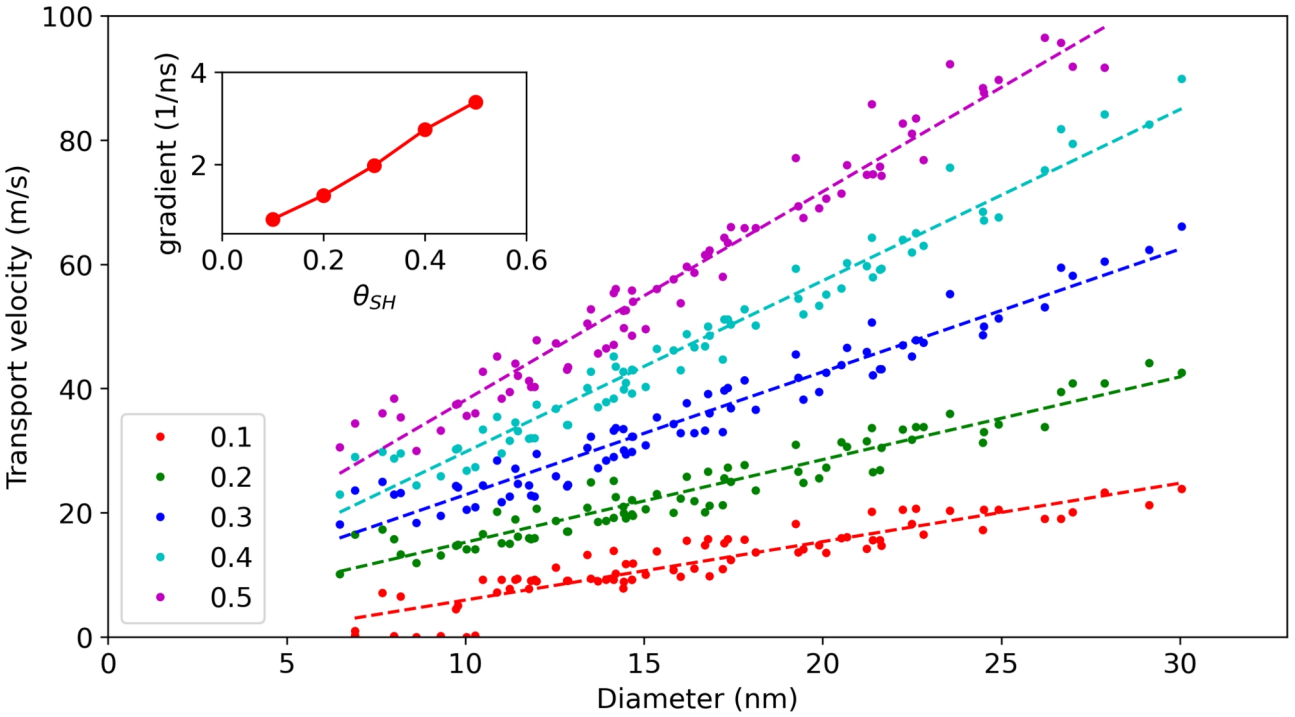

Fig. 4. The relation between skyrmion transport velocity and its diameter under different θ_{SH}. The dotted lines show the result of the linear regression. The gradients from linear regression were shown in the insert.

Skyrmion transport

The generated skyrmions from the above section were then transported using SOT with a current density of $J = 3 \times 10^{11}$ A/m^2. During the transportation process, spin Hall angle θ_{SH}, equivalent to the spin polarisation in Slonczewski spin transfer torque (STT) formulation[70], was varied between 0.1 to 0.5. The resultant transport velocities as a function of skyrmion diameters are shown in Fig. 4. For all θ_{SH}, a general trend that the velocity is proportional to the skyrmion diameter can be observed and confirmed. One might notice the deviation of data points from the linear trend due to the introduced grains which have an inter-grain exchange coupling reduced by 10% as discussed in the methodology section. Linear regressions were carried out for each θ_{SH} data series. The resultant gradients also confirmed the trend of which a larger skyrmion can receive more SOT torque and travel at a higher velocity as expected, posing challenges to minimizing skyrmions.

For the previously reported value $D_{interfacial} = 1.15 \pm 0.57$ mJ/m^2 that is comparable to a Pt/CoFeB system[20], the diameter of the resultant skyrmions would fall below 15 nm as shown in Fig. 3b. For skyrmions radius smaller than 11 nm, at $\theta_{SH} = 0.1$ and current density $J = 3 \times 10^{11}$ A/m^2, some skyrmions gained

Parameter	Value
Landau–Lifshitz damping constant α	0.1
Exchange stiffness A_{ex}	1.0×10^{-11} J/m
Saturation magnetisation M_{sat}	1.0×10^{6} A/m
Uniaxial anisotropy const. K_u	$6.8 \times 10^{5} \mathrm{J/m^3}$
Uniaxial Anisotropy Axis	(0, 0, 1)

Table 1. Simulation parameters[80].

very little momentum with a velocity close to zero. An increase from $\theta_{SH} = 0.1$–0.2 or above can avoid this situation. Since Pt typically has θ_{SH} ranging from 0.03 to 0.10[52–57], the use of β-W as the heavy metal layer can significantly boost skyrmion transport velocity and avoid skyrmions not having enough momentum to move.

Considering the recent development in CMOS transistors, race track memory or logic devices are expected to have a comparable size to the state-of-the-art CMOS transistors of less than 20 nm in width. The grain in velocity for the discussed skyrmion size by enhancing θ_{SH} would be vital to realising and commercializing skyrmion devices. However, one should notice that the skyrmions were unconstrained, unlike race track devices, due to the large mesh in the simulation. The edge of the race track would exert additional dragging force on the skyrmion transport and thus must be taken into account in device design[71,72]. The process of driving the skyrmion might alter the exchange interaction and thus affect the size of the skyrmion indicating more research into the basic aspects of skyrmion transport is needed[73]. For the future aspects of race track devices, there have been proposals of using multiple channels of skyrmion race track[74,75] and multiple layers[76,77] to encode information. Theoretical research into skymionium that has a zero topological charge and thus no skyrmion Hall effect without having to dramatically alter the magnetic properties of the device as suggested in the introduction[33,78]. These devices would surely benefit from a high skyrmion transport velocity from the enhanced θ_{SH}.

Conclusion

To conclude, the generation and transport of skyrmion based on β-W/CoFeB system was studied under different spin Hall angle θ_{SH}. The region of $D_{interfacial}$ and $B_{z,ext}$ has been identified. The later skyrmion transport simulations confirmed a general proportionality between the skyrmion diameter and transport velocity. The confirmation reiterates the difficulties of miniaturising skyrmion devices while maintaining the high transport velocity required for high-performance operation. Fortunately, a clear trend was observed that increasing θ_{SH} can increase the transport velocity providing a way to overcome the skyrmion transport trilemma. For the previously reported $D_{interfacial}$ values of β-W/CoFeB systems, it is likely to form skyrmions in the range of 10–20 nm in diameter based on the findings. In this regime, a considerable gain in velocity compared to a Pt heavy metal layer system can be achieved by the use of β-W. The results provided useful insights into the skyrmion size and transport velocity in β-W/CoFeB system for future experimental work in material and device engineering.

Methods

The simulation parameters of the mesh composed of $1024 \times 1024 \times 1$ cells in the size of $(1 \times 1 \times 1)$ nm can be found in Table 1. In addition, material grains were introduced using Voronoi tessellation[79]. Each region has its uniaxial anisotropy constant Ku scaled by ± 5 %. Exchange coupling between each region was also reduced by 10 %. All simulations were carried out with Nvidia H100 GPUs on the Genkai Supercomputer.

For the skyrmion transport simulation, a spin current with a density of $J = 3 \times 10^{11}$ A/m^2 polarized in the y-direction was injected in the z-direction. The positions of the generated skyrmion between 2.5 and 7.5 ns were used to obtain transport velocities. The first 2.5 ns was neglected to provide a window for the skyrmion to reach its full velocity. Some skyrmions with large diameters went outside the mesh in the 5 ns interval. They would be evaluated between 2.5 and 5 ns or discarded if the velocity is large enough to drive the skyrmion out of the mesh within 5 ns.

It should be noticed that the damping-like torque (DLT) was assumed to be dominant in SOT. Field-like torque (FLT) is not negligible when other materials such as Ta are used as a heavy metal layer, which has a ratio of FLT-to-DLT from 0.7 to 4.0[81–85]. While W has an FLT-to-DLT ratio of about 0.3[86,87], it was assumed that DLT is dominant in this system and FLT is negligible in the simulations for simplicity by setting the Slonczewski secondary STT term ϵ' to zero.

Data Availability

The simulation scripts and data can be found on https://genkai-nextcloud.hpc.kyushu-u.ac.jp/s/bNTaBnJqYSG4x3K.

Received: 19 November 2024; Accepted: 20 February 2025
Published online: 05 March 2025

References

1. Skyrme, T. H. R. A unified field theory of mesons and baryons. *Nuclear Phys.* **31**, 556–569 (1962).
2. Yokouchi, T. et al. Current-induced dynamics of skyrmion strings. *Sci. Adv.* **4**, eaat1115 (2018).

3. Zhang, S. et al. Manipulation of skyrmion motion by magnetic field gradients. *Nat. Commun.* **9**, 2115 (2018).
4. Parkin, S. S., Hayashi, M. & Thomas, L. Magnetic domain-wall racetrack memory. *Science* **320**, 190–194 (2008).
5. Huang, Y., Kang, W., Zhang, X., Zhou, Y. & Zhao, W. Magnetic skyrmion-based synaptic devices. *Nanotechnology* **28**, 08LT02 (2017).
6. Zhang, Z. et al. Skyrmion-based ultra-low power electric-field-controlled reconfigurable (super) logic gate. *IEEE Electron Device Lett.* **40**, 1984–1987 (2019).
7. Zhang, S. et al. Current-induced magnetic skyrmions oscillator. *N. J. Phys.* **17**, 023061 (2015).
8. Nakatani, Y., Yamada, K. & Hirohata, A. Discrimination of skyrmion chirality via spin-orbit and-transfer torques for logic operation. *Sci. Rep.* **11**, 8415 (2021).
9. Crépieux, A. & Lacroix, C. Dzyaloshinsky-moriya interactions induced by symmetry breaking at a surface. *J. Magnetism Magnetic Mater.* **182**, 341–349 (1998).
10. Moriya, T. Anisotropic superexchange interaction and weak ferromagnetism. *Phys. Rev.* **120**, 91 (1960).
11. Lu, J., Li, M. & Wang, X. Quantifying the bulk and interfacial dzyaloshinskii-moriya interactions. *Phys. Rev. B* **101**, 134431 (2020).
12. Tokura, Y. & Kanazawa, N. Magnetic skyrmion materials. *Chem. Rev.* **121**, 2857–2897 (2020).
13. Soumyanarayanan, A. et al. Tunable room-temperature magnetic skyrmions in ir/fe/co/pt multilayers. *Nat. Mater.* **16**, 898–904 (2017).
14. Moreau-Luchaire, C. et al. Additive interfacial chiral interaction in multilayers for stabilization of small individual skyrmions at room temperature. *Nat. Nanotechnol.* **11**, 444–448 (2016).
15. Tolley, R., Montoya, S. & Fullerton, E. Room-temperature observation and current control of skyrmions in pt/co/os/pt thin films. *Phys. Rev. Mater.* **2**, 044404 (2018).
16. Woo, S. et al. Observation of room-temperature magnetic skyrmions and their current-driven dynamics in ultrathin metallic ferromagnets. *Nat. Mater.* **15**, 501–506 (2016).
17. Gerlinger, K. *et al.* Application concepts for ultrafast laser-induced skyrmion creation and annihilation. *Appl. Phys. Lett.* **118** (2021).
18. Denker, C. et al. Size and density control of skyrmions with picometer cofeb thickness variations–Observation of zero-field skyrmions and skyrmion merging. *J. Phys. D Appl. Phys.* **56**, 495302 (2023).
19. Jaiswal, S. *et al.* Investigation of the dzyaloshinskii-moriya interaction and room temperature skyrmions in w/cofeb/mgo thin films and microwires. *Appl. Phys. Lett.* **111** (2017).
20. Böttcher, T. et al. Heisenberg exchange and dzyaloshinskii-moriya interaction in ultrathin pt (w)/cofeb single and multilayers. *IEEE Trans. Magnet.* **57**, 1–7 (2021).
21. Park, Y.-K. et al. Experimental observation of the correlation between the interfacial dzyaloshinskii-moriya interaction and work function in metallic magnetic trilayers. *NPG Asia Mater.* **10**, 995–1001 (2018).
22. Budhani, R. C. et al. Magnetotransport and magnetic textures in ho/fecogd/β-w multilayers. *Phys. Rev. B* **105**, 024412 (2022).
23. Nakata, F., Niimura, T., Kurokawa, Y. & Yuasa, H. Spin seebeck voltage enhancement by mn system metals insertion at the interface between yig and nonmagnetic layer. *Japan. J. Appl. Phys.* **58**, SBBI04 (2019).
24. Heide, M., Bihlmayer, G. & Blügel, S. Dzyaloshinskii-moriya interaction accounting for the orientation of magnetic domains in ultrathin films: Fe/w(110). *Phys. Rev. B* **78**, 140403. https://doi.org/10.1103/PhysRevB.78.140403 (2008).
25. Coester, B. et al. Enhanced spin hall conductivity in tungsten-copper alloys. *J. Magnetism Magnet. Mater.* **523**, 167545 (2021).
26. Saito, Y., Tezuka, N., Ikeda, S. & Endoh, T. Large spin hall effect and increase in perpendicular magnetic anisotropy in artificially synthesized amorphous w/hf multilayer/cofeb system. *Appl. Phys. Lett.* **116** (2020).
27. Yuasa, H., Nakata, F., Nakamura, R. & Kurokawa, Y. Spin seebeck coefficient enhancement by using ta50w50 alloy and yig/ru interface. *J. Phys. D Appl. Phys.* **51**, 134002 (2018).
28. Li, H., Kurokawa, Y., Niimura, T., Yamauchi, T. & Yuasa, H. Composition dependence of spin seebeck voltage in yig/pt100- xrux, pt100- xcux, and pt100- x (cu0. 5ru0. 5) x.. *Japan. J. Appl. Phys.* **59**, 073001 (2020).
29. Woo, S. et al. Spin-orbit torque-driven skyrmion dynamics revealed by time-resolved x-ray microscopy. *Nat. Commun.* **8**, 15573 (2017).
30. Quessab, Y., Xu, J.-W., Morshed, M. G., Ghosh, A. W. & Kent, A. D. Interplay between spin-orbit torques and dzyaloshinskii-moriya interactions in ferrimagnetic amorphous alloys. *Adv. Sci.* **8**, 2100481 (2021).
31. Zhao, Y. et al. Spin-orbit torque driven skyrmion motion under unconventional spin hall effect. *N. J. Phys.* **24**, 053053 (2022).
32. Liu, Y. et al. Voltage-driven high-speed skyrmion motion in a skyrmion-shift device. *Phys. Rev. Appl.* **11**, 014004 (2019).
33. Kolesnikov, A. G., Stebliy, M. E., Samardak, A. S. & Ognev, A. V. Skyrmionium-high velocity without the skyrmion hall effect. *Sci. Rep.* **8**, 16966 (2018).
34. Woo, S., Mann, M., Tan, A. J., Caretta, L. & Beach, G. S. Enhanced spin-orbit torques in pt/co/ta heterostructures. *Appl. Phys. Lett.* **105** (2014).
35. Zhang, W., Han, W., Jiang, X., Yang, S.-H. & SP Parkin, S. Role of transparency of platinum-ferromagnet interfaces in determining the intrinsic magnitude of the spin hall effect. *Nat. Phys.* **11**, 496–502 (2015).
36. Song, C. et al. Spin-orbit torques: Materials, mechanisms, performances, and potential applications. *Progress Mater. Sci.* **118**, 100761 (2021).
37. Wu, H. et al. Ferrimagnetic skyrmions in topological insulator/ferrimagnet heterostructures. *Adv. Mater.* **32**, 2003380 (2020).
38. Zhou, Y., Li, S., Wei, Z., Hou, Z. & Zhou, Y. Room temperature skyrmions in pt/co/gd multilayers and their non-volatile electric-field creation in multiferroic heterostructure. *Appl. Phys. Lett.* **125** (2024).
39. Seung Ham, W. *et al.* Temperature dependence of spin-orbit effective fields in pt/gdfeco bilayers. *Appl. Phys. Lett.* **110** (2017).
40. Caretta, L. et al. Fast current-driven domain walls and small skyrmions in a compensated ferrimagnet. *Nat. Nanotechnol.* **13**, 1154–1160 (2018).
41. Belrhazi, H. & El Hafidi, M. Nucleation and manipulation of single skyrmions using spin-polarized currents in antiferromagnetic skyrmion-based racetrack memories. *Sci. Rep.* **12**, 15225 (2022).
42. Liang, X. et al. Dynamics of an antiferromagnetic skyrmion in a racetrack with a defect. *Phys. Rev. B* **100**, 144439 (2019).
43. Dohi, T., DuttaGupta, S., Fukami, S. & Ohno, H. Formation and current-induced motion of synthetic antiferromagnetic skyrmion bubbles. *Nat. Commun.* **10**, 5153 (2019).
44. Chen, R. et al. Controllable generation of antiferromagnetic skyrmions in synthetic antiferromagnets with thermal effect. *Adv. Functional Mater.* **32**, 2111906 (2022).
45. Qiu, S., Liu, J., Chen, Y., Qi, X. & Fang, L. Writing skyrmion at a specific position in synthetic antiferromagnetic racetrack by voltage. *J. Magnetism Magnet. Mater.* **554**, 169144 (2022).
46. Pai, C.-F. *et al.* Spin transfer torque devices utilizing the giant spin hall effect of tungsten. *Appl. Phys. Lett.* **101** (2012).
47. Hao, Q. & Xiao, G. Giant spin hall effect and switching induced by spin-transfer torque in a $\mathrm{W/co_{40}fe_{40}b_{20}/MgO}$ structure with perpendicular magnetic anisotropy. *Phys. Rev. Appl.* **3**, 034009. https://doi.org/10.1103/PhysRevApplied.3.034009 (2015).
48. Bansal, R., Nirala, G., Kumar, A., Chaudhary, S. & Muduli, P. Large spin hall angle in β-w thin films grown on cofeb without oxygen plasma. In *Spin*, vol. 8, 1850018 (World Scientific, 2018).
49. Sui, X. et al. Giant enhancement of the intrinsic spin hall conductivity in β-tungsten via substitutional doping. *Phys. Rev. B* **96**, 241105 (2017).
50. Demasius, K.-U. et al. Enhanced spin-orbit torques by oxygen incorporation in tungsten films. *Nat. Commun.* **7**, 10644 (2016).
51. Fulara, H. et al. Spin-orbit torque-driven propagating spin waves. *Sci. Adv.* **5**, eaax8467 (2019).

52. Wang, Y., Deorani, P., Qiu, X., Kwon, J. H. & Yang, H. Determination of intrinsic spin hall angle in pt. *Appl. Phys. Lett.* **105** (2014).
53. Saito, Y., Tezuka, N., Ikeda, S., Sato, H. & Endoh, T. Spin hall effect investigated by spin hall magnetoresistance in pt100- xaux/cofeb systems. *AIP Adv.* **9** (2019).
54. Ando, K. et al. Electric manipulation of spin relaxation using the spin hall effect. *Phys. Rev. Lett.* **101**, 036601 (2008).
55. Wang, H. et al. Scaling of spin hall angle in 3d, 4d, and 5d metals from y 3 fe 5 o 12/metal spin pumping. *Phys. Rev. Lett.* **112**, 197201 (2014).
56. Ando, K. *et al.* Inverse spin-hall effect induced by spin pumping in metallic system. *J. Appl. Phys.* **109** (2011).
57. Hahn, C. et al. Comparative measurements of inverse spin hall effects and magnetoresistance in yig/pt and yig/ta. *Phys. Rev. B* **87**, 174417. https://doi.org/10.1103/PhysRevB.87.174417 (2013).
58. Lee, J. et al. Ti-alloyed β-w heterojunctions exhibiting spin-orbit torque switching at a wide operating temperature range. *Appl. Surface Sci.* **682**, 161671 (2025).
59. Lu, S. *et al.* Enlarged thickness window and maintained high spin–orbit torque efficiency for metastable tungsten by increasing amorphous crystalline: A path toward low-power mram. *ACS Appl. Electronic Mater.* (2024).
60. Shao, Q. et al. Roadmap of spin-orbit torques. *IEEE Trans. Magnetics* **57**, 1–39 (2021).
61. Vansteenkiste, A. et al. The design and verification of Mumax3. *AIP Adv.* **4**, 107133. https://doi.org/10.1063/1.4899186 (2014).
62. Finocchio, G., Büttner, F., Tomasello, R., Carpentieri, M. & Kläui, M. Magnetic skyrmions: From fundamental to applications. *J. Phys. D Appl. Phys.* **49**, 423001 (2016).
63. Birch, M. et al. Real-space imaging of confined magnetic skyrmion tubes. *Nat. Commun.* **11**, 1726 (2020).
64. Karube, K. et al. Robust metastable skyrmions and their triangular-square lattice structural transition in a high-temperature chiral magnet. *Nat. Mater.* **15**, 1237–1242 (2016).
65. Tang, J. et al. Magnetic skyrmion bundles and their current-driven dynamics. *Nat. Nanotechnol.* **16**, 1086–1091 (2021).
66. Lee, K.-M., Choi, J. W., Sok, J. & Min, B.-C. Temperature dependence of the interfacial magnetic anisotropy in w/cofeb/mgo. *AIP Adv.* **7** (2017).
67. Wang, X., Yuan, H. & Wang, X. A theory on skyrmion size. *Commun. Phys.* **1**, 31 (2018).
68. Liu, Q. et al. Room-temperature creation and conversion of individual skyrmion bags in magnetic multilayered disks. *Nat. Commun.* **16**, 125 (2025).
69. Qin, Z. et al. Size-tunable skyrmion bubbles in ta/cofeb/mgo multilayers. *J. Phys. D Appl. Phys.* **51**, 425001 (2018).
70. Joos, J. J. *et al.* Tutorial: Simulating modern magnetic material systems in mumax3. *J. Appl. Phys.* **134** (2023).
71. Al Saidi, W. *et al.* Control of skyrmions in confined devices for multistate memory application. *Physica Status Solidi (a)*. 2400489 (2024).
72. Chen, X. *et al.* Skyrmion dynamics in width-varying nanotracks and implications for skyrmionic applications. *Appl. Phys. Lett.* **111** (2017).
73. Iwasaki, J., Mochizuki, M. & Nagaosa, N. Universal current-velocity relation of skyrmion motion in chiral magnets. *Nat. Commun.* **4**, 1463 (2013).
74. Song, C. *et al.* Skyrmion-based multi-channel racetrack. *Appl. Phys. Lett.* **111** (2017).
75. Müller, J. Magnetic skyrmions on a two-lane racetrack. *N. J. Phys.* **19**, 025002 (2017).
76. Chen, R. et al. Encoding and multiplexing information signals in magnetic multilayers with fractional skyrmion tubes. *ACS Appl. Mater. Interfaces* **15**, 34145–34158 (2023).
77. Suess, D., Vogler, C., Bruckner, F., Heistracher, P. & Abert, C. A repulsive skyrmion chain as a guiding track for a racetrack memory. *AIP Adv.* **8** (2018).
78. Göbel, B., Schäffer, A. F., Berakdar, J., Mertig, I. & Parkin, S. S. Electrical writing, deleting, reading, and moving of magnetic skyrmioniums in a racetrack device. *Sci. Rep.* **9**, 12119 (2019).
79. Mulkers, J., Van Waeyenberge, B. & Milošević, M. V. Effects of spatially-engineered Dzyaloshinskii-Moriya interaction in ferromagnetic films. *Phys. Rev. B* **95**, 144401. https://doi.org/10.1103/PhysRevB.95.144401 (2017).
80. Yang, S. et al. Electrical generation and deletion of magnetic skyrmion-bubbles via vertical current injection. *Adv. Mater.* **33**, 2104406. https://doi.org/10.1002/adma.202104406 (2021).
81. Fan, W. et al. Asymmetric spin-orbit-torque-induced magnetization switching with a noncollinear in-plane assisting magnetic field. *Phys. Rev. Appl.* **11**, 034018 (2019).
82. Lee, J. M. et al. Oscillatory spin-orbit torque switching induced by field-like torques. *Commun. Phys.* **1**, 2 (2018).
83. Kim, J. et al. Layer thickness dependence of the current-induced effective field vector in ta| cofeb| mgo. *Nat. Mater.* **12**, 240–245 (2013).
84. Torrejon, J. et al. Interface control of the magnetic chirality in cofeb/mgo heterostructures with heavy-metal underlayers. *Nat. Commun.* **5**, 4655 (2014).
85. Qiu, X. et al. Angular and temperature dependence of current induced spin-orbit effective fields in ta/cofeb/mgo nanowires. *Sci. Rep.* **4**, 4491 (2014).
86. Vudya Sethu, K. K. et al. Optimization of tungsten β-phase window for spin-orbit-torque magnetic random-access memory. *Phys. Rev. Appl.* **16**, 064009 (2021).
87. Krizakova, V. et al. Tailoring the switching efficiency of magnetic tunnel junctions by the fieldlike spin-orbit torque. *Phys. Rev. Appl.* **18**, 044070 (2022).

Acknowledgements

This work was supported by JSPS KAKENHI (Grant numbers JP22KK0056, JP23K22827, JP24H00030,-JP24H02235), MEXT Initiative to Establish Next-Generation Novel Integrated Circuit Centers (X-NICS), TheCenter for Spintronics Research Network (Osaka), UPWARDS for the future. Simulations were performedusing the computing resources offered under the category of General Projects by the Research Institute forInformation Technology, Kyushu University. L.Z. was partially supported by the Establishment of UniversityFellowships Towards the Creation of Science and Technology Innovation, Grant no. JPMJFS2132.

Author contributions

T.C.C. carried out the simulations, analysed the results and wrote the manuscript, L.Z. wrote part of the introduction, Y.K, K.T and H.Y. provided comments on the simulation approach, and R.S. wrote the initial version of the simulation code.

Declarations

Competing interests

The authors declare no competing interests.

Additional information

Supplementary Information The online version contains supplementary material available at https://doi.org/10.1038/s41598-025-91415-z.

Correspondence and requests for materials should be addressed to T.C.C.

Reprints and permissions information is available at www.nature.com/reprints.

Publisher's note Springer Nature remains neutral with regard to jurisdictional claims in published maps and institutional affiliations.